Three-dimensional biofabrication of nanosecond laser micromachined nanofibre meshes for tissue engineered scaffolds

Ross H. McWilliam[1], Wenlong Chang[2], Zhao Liu[3], Jiayuan Wang[3], Fengxuan Han[3], Richard A. Black[1], Junxi Wu[1], Xichun Luo[2], Bin Li[3], Wenmiao Shu[1,]*

Key Words:
3D biofabrication; electrospinning; hierarchical scaffold; micromachining; tissue engineering

From the Contents

Introduction	104
Methods	105
Results	108
Discussion	110

ABSTRACT

There is a high demand for bespoke grafts to replace damaged or malformed bone and cartilage tissue. Three-dimensional (3D) printing offers a method of fabricating complex anatomical features of clinically relevant sizes. However, the construction of a scaffold to replicate the complex hierarchical structure of natural tissues remains challenging. This paper reports a novel biofabrication method that is capable of creating intricately designed structures of anatomically relevant dimensions. The beneficial properties of the electrospun fibre meshes can finally be realised in 3D rather than the current promising breakthroughs in two-dimensional (2D). The 3D model was created from commercially available computer-aided design software packages in order to slice the model down into many layers of slices, which were arrayed. These 2D slices with each layer of a defined pattern were laser cut, and then successfully assembled with varying thicknesses of 100 μm or 200 μm. It is demonstrated in this study that this new biofabrication technique can be used to reproduce very complex computer-aided design models into hierarchical constructs with micro and nano resolutions, where the clinically relevant sizes ranging from a simple cube of 20 mm dimension, to a more complex, 50 mm-tall human ears were created. In-vitro cell-contact studies were also carried out to investigate the biocompatibility of this hierarchal structure. The cell viability on a micromachined electrospun polylactic-co-glycolic acid fibre mesh slice, where a range of hole diameters from 200 μm to 500 μm were laser cut in an array where cell confluence values of at least 85% were found at three weeks. Cells were also seeded onto a simpler stacked construct, albeit made with micromachined poly fibre mesh, where cells can be found to migrate through the stack better with collagen as bioadhesives. This new method for biofabricating hierarchical constructs can be further developed for tissue repair applications such as maxillofacial bone injury or nose/ear cartilage replacement in the future.

http://doi.org/10.12336/biomatertransl.2023.02.005

How to cite this article:
McWilliam, R. H.; Chang, W.; Liu, Z.; Wang, J.; Han, F.; Black, R. A.; Wu. J.; Luo, X.; Li, B.; Shu, W. Three-dimensional biofabrication of nanosecond laser micromachined nanofibre meshes for tissue engineered scaffolds. *Biomater Transl.* **2023**, *4*(2), 104-114.

Introduction

Bone and cartilage are examples of tissue that are both capable of being distinctly and prominently shaped whilst being prone to injury and damage. Injuries and abnormalities to the bone and cartilage such as microtia and anotia of the ear and tumour removal are a prevalent problem facing health services.[1-8] Taking anotia and microtia (where the ear cartilage either does not or only partly develops *in utero*) as an example, a global study covering the years 1988 to 2007, the prevalence stands at approximately 2.06 cases per 10,000 neonatal patients,[9] and the current treatment of autografting a shaped costal cartilage graft requires several invasive surgeries and a risk of donor site morbidity.[10] Additionally, over 500,000 bone graft surgeries were performed annually in the USA.[11] Current treatments for

maxillofacial bone repair require either autografting pelvic bone, an invasive surgery with the risk of donor site morbidity, or metal plate implants, which are uncomfortable, prone to wear or based on more costly titanium alloys.[12, 13]

These current treatments can be improved upon greatly using biomaterials and processes that are more compatible with native tissue and development.[5, 14-16] Electrospinning, where fibre meshes are created by using a potential difference to draw a polymer from a source – such as in a solvent solution – to a collector, is one such technique regarded as producing a fine nanofiber mesh.[17, 18] Both natural and synthetic polymer fibre meshes can be fabricated, and studies have shown that they have advantageous properties with regards to cell viability, response and differentiation due to their resemblance to tissue extracellular membrane (ECM).[19] However, the main difficulty of electrospinning and bone and cartilage repair is to scale up the process in three-dimensional (3D) and fabricate a precise 3D structure with clinically relevant dimensions.[20] To this end, melt electrowriting is one technique that combines electrospinning with additive manufacturing and is capable of producing 3D structures of fibre meshes with unprecedented micro and nanoscale precision. The polymer filaments are drawn from the molten polymer instead of a solvent dispersion, and directly deposited on the substrate under the action of electrostatic forces. Fabrication thickness is still limited to achieve any clinically relevant sizes due to the deteriorated electrical field for thicker constructs.[21-24]

The technique of 3D bioprinting, on the other hand, offers a means of fabricating bespoke, clinically relevant sized, hierarchal structures.[25-30] This technique involves the use of cells and a specifically designed biomaterial scaffold to fabricate a 3D hierarchal graft, which can be scaled to clinically relevant sizes according to a patient's specific anatomical structure.[31, 32] However, the main challenge of 3D bioprinting is the ability to print the scalable sizes that can be self-supportive whilst using materials that resemble the ECM. Currently, it is difficult to achieve a 3D bioprinted structure having both adequate biological and mechanical function.[33]

In an attempt to overcome these problems, electrospun fibre meshes have been proposed.[34-36] One recent approach involves stacking two-dimensional (2D) layers of electrospun mesh and 3D printed discs on top of each other to make a 3D shape.[37] While the methodology implemented in these studies has shown promising results *in vitro*, there is scope for improvements to be made in order to biofabricate patient specific constructs at scale and having clinically relevant dimensions.

To date, there it has been challenging to mimic faithfully the 3D hierarchical structures that make up complex human tissue.[38] Any novel fabrication method must take into account the macro scale to match the clinically relevant size of the tissue being replaced, the microscale precision for the anatomic shape and to allow cell migration and accurate ECM formation, and nanoscale precision for the morphological resemblance to ECM to maximise native cell viability and performance.[39, 40]

In this paper, we report a novel method for 3D biofabricate tissue scaffolds with microscale precision from nanofibrous materials. The method involves stacking 2D nanofibre meshes that have been laser cut into distinct cross-sectional shapes in a prescribed sequence, the position and orientation of each slice being specified to achieve an accurate representation of the anatomical feature. The stacked nanofibrous meshes alone would not allow cell migration through each slice, something that would be an issue for the potential success of any graft where cells are required to be uniformly dispersed, due to the lack of microporosity within the nanofiber meshes; this also hinders nutrient diffusion to cells within the construct and the potential for vascularisation, vital for ensuring cell survival and thus the success of the graft. Using a nanosecond laser cutter to micromachine arrays of circular voids of different diameters into fibre meshes have already been shown to support cell growth and proliferation.[41, 42] Equally important is the length scale and interconnectivity of the voids, to ensure that cells are uniformly dispersed through the structure at the time of seeding, and that once attached those cells are able to proliferate throughout the structure and deposit ECM, thereby consolidating the tissue scaffold and ensuring effective engraftment to the surrounding host tissue.[43] Using this novel method various designs were successfully fabricated with good accuracy and with application relevant sizes and cosmetics, ranging from some simple shapes up to realistic, anatomically relevant body parts such as a human ear.

The aim of the present study is to explore further the potential of micromachining techniques to optimise the microporosity and performance of such 3D constructs *in vitro*.

Methods

Scaffold fabrication

The polycaprolactone (PCL) nanofiber mesh from which the cell scaffolds were fabricated was produced in sheet form using a bespoke electrospinning apparatus at the University of Strathclyde.[44] PCL pellets (molecular weight = 80,000; Sigma-Aldrich, Gillingham, UK) were dissolved in a 9:1 mixture of acetone and dimethyl formamide (DMF; both from Sigma-Aldrich) to a final concentration of 17 wt%. The polymer dispersion was delivered from a 5 mL syringe (Sigma-Aldrich) fitted with a 20G gauge needle (Vicson, UK) at a flow rate of 2 mL/h. The electrostatic potential was set at –15 kV. The polylactic-co-glycolic acid (PLGA) nanofibre mesh was kindly donated by The Electrospinning Company Ltd. (Oxfordshire, UK).

*Corresponding author: Wenmiao Shu, will.shu@strath.ac.uk.

1 Department of Biomedical Engineering, University of Strathclyde, Glasgow, UK; 2 Centre for Precision Manufacturing, Design, Manufacturing & Engineering Management, University of Strathclyde, Glasgow, UK; 3 Orthopaedic Institute, Department of Orthopaedic Surgery, The First Affiliated Hospital, Soochow University, Suzhou, Jiangsu Province, China

Design and three-dimensional construction of scaffold

In order to ensure an accurate 3D reconstruction, stacking method was devised to facilitate the layer-by-layer assembly of each slice in the correct sequence. This method can be described as using a square, acrylic base with four tall steel pins in each corner, each 3 mm in diameter, to guide the alignment of each slice (a sheet that has been cut using a CO_2 laser, a square that is the same dimensions as the base, and with a 3 mm hole in each corner orientated exactly in line with the pins). In this way, having successfully positioned the individual sections, one on top of the other, the full 3D reconstruction may be realised.

A computer model of the desired shape (for the purpose of proving the concept of a cube, a hemisphere, a pyramid and an ear, all of varying sizes) was constructed in computer aided design (CAD) software (Inventor® Version 2018, Autodesk, Dublin, Ireland), to which four 3 mm cylinders (corresponding to the pins) and an enclosure (corresponding to the base) were added. A 1-mm thick support structure was added to locate the shape of the surrounding enclosure. A rendered view of the final 3D model is shown in **Figure 1A**. This model was saved as a stereolithography (stl) file and opened in Slicer (Version 1.3.0 GNU Affero), a slicing software often utilised for 3D printing (additive manufacturing). Thereafter, the file was exported in the open standard scalable vector graphic (svg) file format, in which the layer thickness is specified by the user and the model is sliced horizontally into layers, each having this well-defined thickness. The model was then imported into Inkscape (version 0.92 GNU General Public Licence), in which the model was further processed to yield an array of slices having the appropriate dimensions (a sample of an 'ungrouped' and arrayed svg is shown in **Figure 1B**). Each slice was then numbered (to help with the construction process later) and saved as a drawing exchange format (dxf) file for laser cutting by a TMX65 50 W CO_2 laser (CTR Lasers, Northampton, UK). **Figure 1C** shows an example of the electrospun polymer sheet after processing by the laser, complete with 3-mm diameter alignment holes at each corner, while **Figure 1D** shows an example of the layers from which the part is to be constructed.

In order to ensure an accurate 3D reconstruction of the laser cut-outs, a stacking method was devised to facilitate the layer-by-layer assembly of each slice in the correct sequence on a custom-made jig. The jig was fabricated in acrylic from a block 55 mm × 55 mm in size and fitted with four stainless steel pins, each 3 mm in diameter (**Figure 1E**). In this way, having successfully positioned the individual sections, one on top of the other, the full, 3D reconstruction of the desired shape could be realised.

For the purpose of demonstrating the technique, two grades of filter paper (Cat 50 and Cat 40, respectively; GE Whatman, Buckinghamshire, UK) were used. The former had a nominal thickness of 100 μm and the latter 200 μm.

Once the shapes had been cut out of the material by the laser, they were assembled as described above and bound together with a 4% aqueous solution of sodium alginate (Sigma-Aldrich). In **Figure 1E**, step 1, the correctly numbered laser cut slice is slotted onto the alignment base. Step 2 shows the application of the alginate via a needle and syringe (alternatively, the solution was dispensed from a bioprinting nozzle). In step 3 the corresponding construct slice is adhered to the preceding construct slice in the correct position and orientation as dictated by the alignment slice. Steps 4 and 5 show how the process repeats itself until all the slices have been laid onto the structure. Thereafter, the 3D construct was immersed in a calcium chloride solution (100 mM) to cross-link the alginate and strengthen the structure. Finally, the alignment slices were removed carefully from the alignment base, leaving only the desired structure standing on the base. In a further experiment, above steps were repeated with collagen instead of alginate in step 2 of **Figure 1E** and thermally cross-linking in a 37°C incubator for 1 hour.

Morphological analysis of the polycaprolactone nanofibre mesh

A scanning electron microscope (SEM) image was taken of a typical PCL electrospun fibre mesh using a Hitachi TM-1000 Desktop SEM Machine (Chiyoda, Japan). From this image, the diameters of ten random fibres were measured using ImageJ (version 1.53e; National Institutes of Health, Bethesda, MD, USA), and an average was taken. Ten randomly selected pores were then measured (also with ImageJ) for their area and the length at their narrowest point. This is to determine if there is a possibility for cell mobility through the nanofiber mesh.

***In vitro* studies**

Cell-contact studies: cell viability

Murine adipose derived stem cells (ADSCs) were kindly donated by researchers at the University of Glasgow, UK. Cells were cultured using minimal essential media (MEM; Gibco, Thermofisher Scientific, Inchinnan, UK) containing 10% fetal bovine serum (Gibco, Thermofisher Scientific) and and 1% penicillin/streptomycin (Corning, Thermofisher Scientific), in an incubator set at 37°C and 5% CO_2 atmosphere.

Micromachined two-dimensional slice

An *in-vitro* cell-contact study was performed on individual micromachined PLGA sheets in order to understand whether the application of an appropriate cell type, in this case, ADSCs, which have the potential to differentiate into osteoblasts after they have become attached to and proliferated on such a 2D construct. Here, a V2-1-100-20-20 nanosecond laser (IPG Photonics, Coventry, UK) was used to cut an array of holes of varying sizes in the range 200, 300, 400, and 500 μm. The diameter of the holes that were made in the PLGA sheets was verified by direct measurement using a Brunel SP50 light microscope (Chippenham, UK). ImageJ was used to measure the average diameter of each hole sampled by taking three measurements for each hole and taking an average. Three holes for each sample were then measured and the average hole diameter for that array was calculated.

The samples were sterilised in a 70% ethanol solution for 1 hour, and washed three times with phosphate buffered saline (Gibco, Thermofisher Scientific), after which 200,000 ADSCs were seeded onto each array. For live/dead staining, the samples were stained with fluorescein and propidium iodide at day 21 to assess cell growth and viability, and then viewed under an inverted epifluorescent microscope (Nikon Eclipse TE300 Epifluorescent inverted microscope, Minato city, Tokyo, Japan).

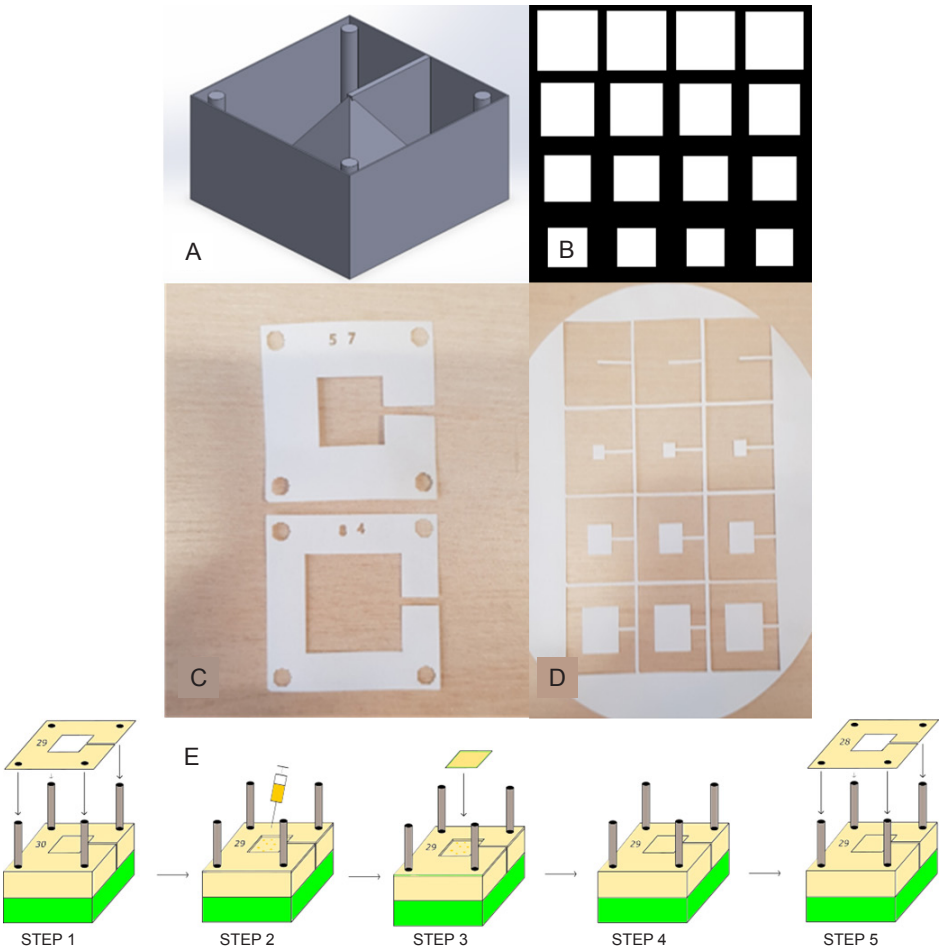

Figure 1. Design and assembly process for fabricating a 3D construct. (A) CAD model with 3D construction and surrounding box and cylinders. (B) Section of the array in InkScape showing different 2D slice shapes used to construct the pyramid. (C) Laser cut alignment slices with an appropriate number designating order. (D) Shape slices on the bulk material to be cross-referenced with alignment slice and placed accordingly on the construct. (E) Schematic of the steps involved in the assembly process, where accurate 3D reconstructions can be created from the 2D slices: Step 1 – placement of alignment slice 29 on the rig using the four holes; Step 2 – Deposition of a couple of drops of alginate solution using a syringe; Steps 3 and 4 – placement of the appropriate shape slice corresponding with alignment slice 29; Step 5 – starting the process again with alignment slice 28. This process continues until all slices are placed. 2D: two-dimensional; 3D: three-dimensional; CAD: computer-aided design. Created with Inventor® Vension 2018.

Prior to this, a 7-day cytotoxicity study was performed using the same number of ADSCs on a 500 μm micromachined PLGA mesh. This sample was stained with fluorescein and propidium iodide and imaged using a Zoe Microscope (Bio-Rad, Hertfordshire, UK).

Micromachined three-dimensional construct

A direct cell-contact study was also conducted in order to determine the cell viability, migration and proliferation throughout a structure according to the methods detailed as above. The cells used in this experiment were ADSCs. The structures in this case are to be far simpler than those made with the paper, with a micromachined electrospun PCL fibre mesh to be used instead and will be a short cylinder using three stacked 14 mm diameter discs. This is so that they can fit neatly into a 24-well plate well. Before assembly the discs were micromachined using the nanosecond laser, to produce circular voids 500 μm in diameter, with a 1 mm pitch. This void size, which is comparable to that of cancellous bone, has been found previously in this study (Section 'Morphological assessment of micromachined fibre meshes') to promote good cell viability. The average pore diameter was calculated by taking three diameter measurements and calculating the average, to be compared with the intended diameter of 500 μm.

The discs were sterilised using a solution of 70% ethanol, dried sufficiently and washed three times with PBS. Each structure was made using three discs, adhered together using 4% sodium alginate crosslinked by calcium chloride, then placed in a 24-well plate well. They were stacked (and this is consistent with all experimentation in the same manner) randomly on top of each other. ADSCs were then seeded onto the structure at a density of 1×10^6, then submerged in culture media.

The discs were stained with fluorescein and propidium iodide at two time points (1 and 7 days; $n = 2$) to assess cell growth and viability. In order to test the perfusion of the cells each of the layers were delaminated and viewed under an inverted epifluorescent microscope.

The above methodology was repeated using collagen as the binding agent instead of alginate. Type 1 collagen (rat tail, , 3 mg/mL, Sigma-Aldrich) was prepared of which 0.5 mL was used to prepare each stack, comprising three layers, which were left for 1 hour in an incubator to gel (cross link). The cells were seeded at a density of 3×10^6 cells per sample stack. Cell viability was assessed at days 1 and 4 ($n = 2$).

Results

Construction of three-dimensional demonstrators

Using the method, 3D constructs of the following shapes were created: a simple cube, with dimensions 20 mm in each direction (**Figure 2A**); a pyramid made from 77 slices with a 20 mm square base and 21.6 mm tall (**Figure 2B**); and a hemisphere 15 mm in diameter (**Figure 2C**). The latter shape was fabricated in different sizes to verify the dimensional accuracy of the construction process and with a view to producing more complex anatomic structures, in this case, a life size model of the human ear (**Figure 2D**).

Finally, a life-sized model of the human ear was fabricated (approximately 50 mm in height) but the paper used was 100 μm, half the thickness of the layer height of the previous ears and shapes constructed. The intention of using thinner layers of paper was to produce a smoother structure, where smaller features can be more pronounced and accurately represented. The result reflected the intention behind this move, where the ear looks better and is shown in **Figure 2E**.

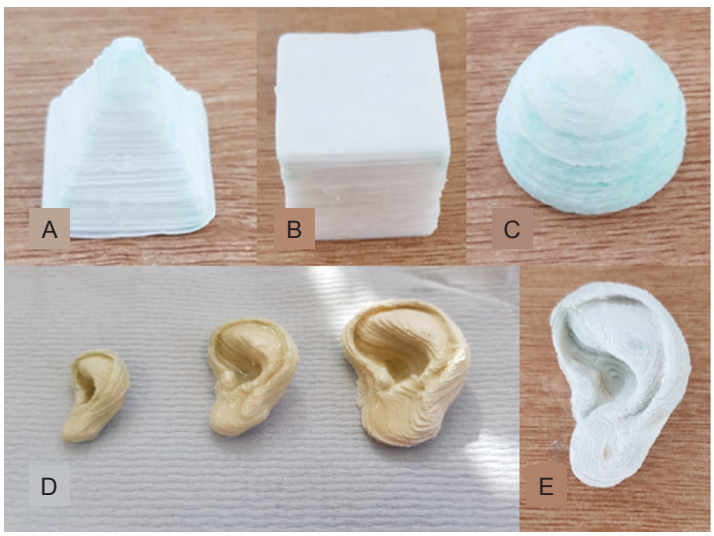

Figure 2. Examples of 3D demonstrators assembled according to the novel fabrication method. (A) Camera image of a pyramid. (B) Camera image of a successfully printed cube. (C) Camera image of a successfully printed hemisphere. (D) Three scale models of a human ear (200 μm slices) of three different sizes. (E) The corresponding ear with greater resolution (100 μm slices), which has excellent fidelity for anatomical size and accurately replicates the complex features of the human ear. Scale bars: 10 mm (A–C, E), 50 mm (D).

Morphological assessment of micromachined fibre meshes

Figure 3 shows the SEM image of a PCL electrospun nanofibre mesh that would be used in coming studies. The clear nanofibre formation shows the effectiveness of the electrospinning process. The average fibre diameter was measured to be 1.801 ± 0.411 μm. The average pore area was found to be 28.612 ± 10.07 μm^2, where their corresponding 'narrowest pore diameter' is 4.542 ± 1.159 μm.

The first micromachining test and the cytotoxicity test showed excellent results. The micromachined hole is close to a circle in shape and the hole is cut completely through the mesh, thus showing the necessity of using the nanosecond laser (**Figure 4A**). The live/dead stain shows excellent cell viability on this micromachined mesh (**Figure 4B**).

Figure 4C–F shows the light microscope images of the PLGA nanofibre meshes post-micromachining, in order from 200 to 500 μm hole diameters respectively. The holes imaged have good circularity and the difference in diameter can be seen visually when comparing these images. **Figure 4G–J** shows the live/dead staining images of the micromachined mesh with the varying hole sizes at the time-point week 3, with alive ADSCs shown as green. All samples have good cell viability, with plenty of green cells and almost no dead cells to be seen.

Viability of cells seeded in polycaprolactone and polylactic-co-glycolic acid three-dimensional scaffolds

Figure 4K–M shows the light microscope images of an array of perforations on three different samples of PCL electrospun mesh material, while **Figure 5** details the diameter of each hole. The stack samples for the *in vitro* experiment were created successfully as per the methodology, and the cells were seeded on the top of each stack.

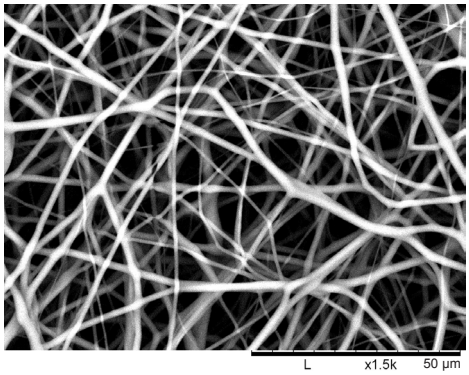

Figure 3. Desktop scanning electron microscope image of an electrospun polycaprolactone nanofibre mesh to be micromachined and used in *in vitro* testing. An average nanofibre diameter was 1.801 µm (n = 10) was found. Scale bars: 50 µm.

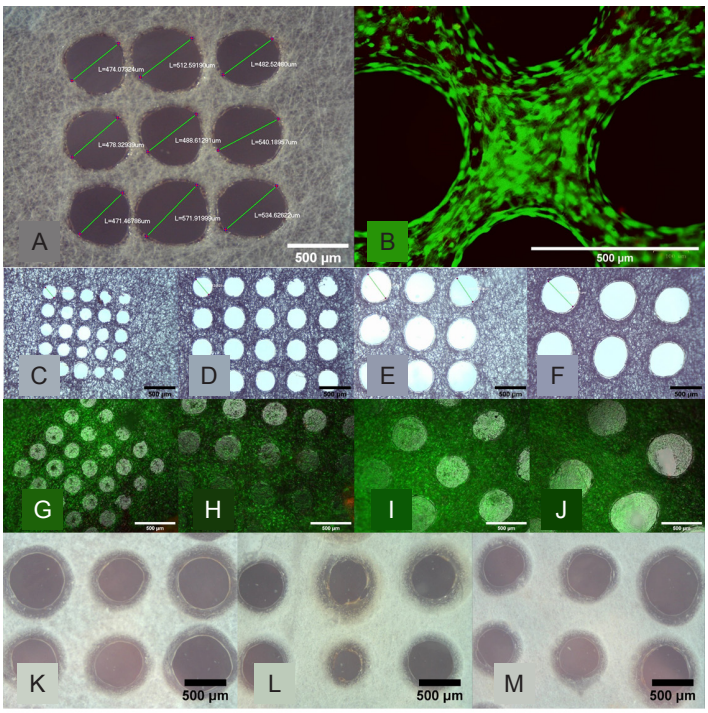

Figure 4. Morphological assessment of the perforated micromachined fibre mesh. (A, B) First cytotoxicity test of the 500 µm micromachined PLGA mesh. (A) Light Microscopy image of the micromachined array showing good circularity. (B) Live/dead image showing excellent cell viability and the holes clearly defined. (C–F) Light microscopy images of the 200 (C), 300 (D), 400 (E), and 500 (F) µm hole arrays, which show good circularity and even distribution. (G–J) Epifluorescent microscope images of live ADSCs on the micromachined fibre mesh with 200 (G), 300 (H), 400 (I), and 500 (J) µm hole arrays, with excellent cell viability seen across all samples, and 'bridging' of cells across. (K–M) Light microscope images of three selected micromachined electrospun PCL fibre mesh samples, all micromachined with the same setting but with minor variances as a result of the non-uniform thickness of the PCL nanofibre mesh. Scale bars: 500 µm. PCL: polycaprolactone; PLGA: polylactic-co-glycolic acid.

Figure 6 shows the live/dead images obtained on the slices from the alginate and the collagen stacks constructed. At two time points (days 1 and 7) slices 1, 2 and 3 on the alginate stacks are being compared with slices 1, 2 and 3 from the collagen stacks. It can be seen from the alginate stacks (**Figure 6A–F**) that there are surviving cells on the top slices at each time point (**Figure 6A** for day 1 and **Figure 6D** for day 7), but that there are no live cells on slices 2 and 3 even after 14 days. The opposite however can be said of the collagen stacks of which the live/dead images are shown in **Figure 6G–L**), where even after 1 day live cells can be seen on the lower stacks (**Figure 6I**).

This confirms the hypothesis that the alginate does not aid in cell migration whereas the collagen does. Therefore, it can be said that the collagen provides a better biological response to the alginate as an adhesive. Cell counting analysis, which quantifies the data from **Figure 6** by showing the live number of cells on each slice by using ImageJ software, also reinforces this data. It can be seen that the number of cells on the lower slices on the alginate stacks (blue columns) is far fewer than those on the collagen stacks (red columns), regardless of the time point.

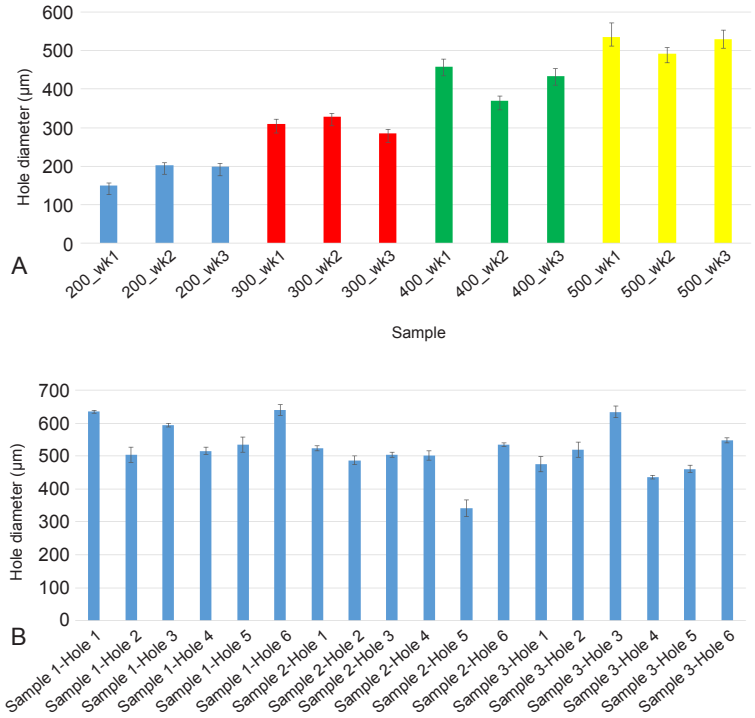

Figure 5. The average diameter of the micromachined perforations in the electrospun fibre mesh samples. (A) The actual average hole diameter of each array (n = 3 holes) compared to the intended hole diameter of the PLGA samples, where the average diameter can be seen to be close to the intended diameter and a clear difference between each sample type seen. (B) The average diameter of each hole (n = 3 holes) in three representative micromachined electrospun PCL fibre mesh samples, with a wider variance of values around the intended 500 μm hole diameter due to using the same laser settings on the non-uniform thickness of the PCL nanofibre mesh. 3D: three-dimensional; PCL: polycaprolactone; PLGA: polylactic-co-glycolic acid.

Discussion

Construction of three-dimensional demonstrators

One of the first issues was that (apart from the cube which has the same cross section throughout the structure) it is difficult to ensure that the construct slice is placed with the correct alignment slice. The way this issue was resolved by adding a thin connection on the CAD model between the intended construct and the outside alignment (**Figure 1A**). This is then seen as a thin connection between the construct slice to the extraneous parts of the paper sheet (as shown in **Figure 1D**). This can be identified as associating with the correct numbered alignment slice which has been completely cut away (**Figure 1C**). The removal of the alignment slices from the construct upon completion of the stacking process[45] was performed carefully in order to prevent delamination and construct deterioration.

It was expected that the process of using crosslinked alginate would swell the construct in the z direction, so that the actual height of the construct would be different from that of the expected height (the number of slices multiplied by the height of each slice).[46] **Table 1** shows the ratio between the expected height and the actual height for the cube, the pyramid and the hemisphere. If an average of the three ratios are taken (found to be 1.38) then the number of slices of future slices can be adjusted to ensure that the height is accurate to that of the CAD model and not swelled due to the alginate. This adjustment was implemented when using a slicer (sliced to svg using 276 μm layer height instead of 200 μm for example).

Table 1. Actual versus the predicted height of the cube, pyramid and hemisphere, along with the ratio of the discrepancy

Shape	Expected height (mm)	Actual height (mm)	Ratio
Cube	18.00	24.77	1.376
Hemisphere	12.60	16.87	1.350
Pyramid	15.40	21.62	1.404

Note: These values are fairly close together, and so can be used to determine that a swelling coefficient of 1.38 should be used for future prints to ensure accurate z-axis fidelity.

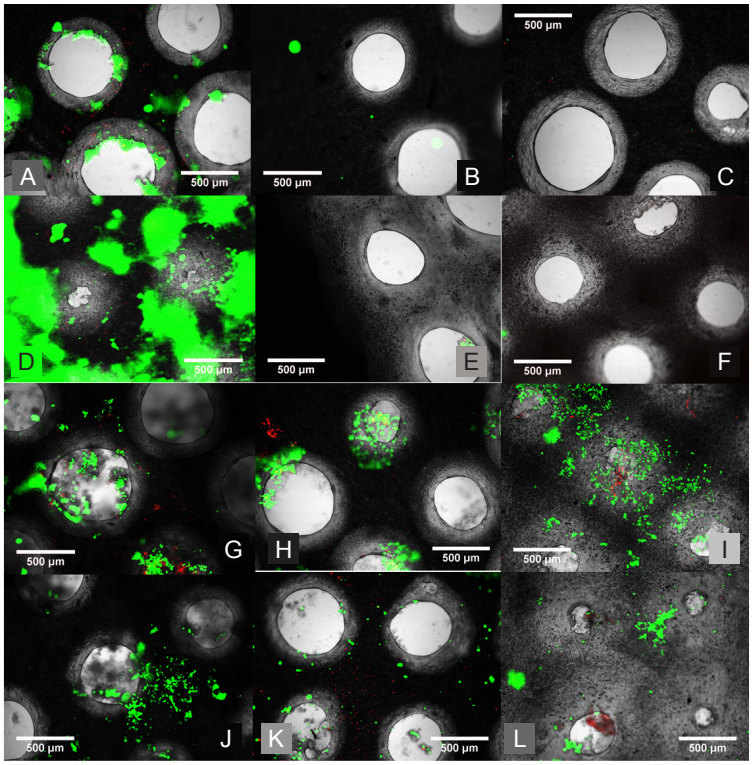

Figure 6. Live/dead staining of ADSCs on the alginate and collagen stacks. (A–F) Inverted epifluorescent microscope images after live/dead staining of ADSCs on the alginate stacks. (A) Slice 1 (top slice) showing some good cell viability on day 1. (B) Slice 2 (middle slice) showing very limited cell presence indicating no cell mobility through the construct on day 1. (C) Slice 3 (bottom slice) showing no cells and thus no mobility through the cross-linked alginate on day 3. (D) Slice 1 (top slice) showing good cell viability with some stain intake by the alginate on day 7. (E) Slice 2 (middle slice) showing limited cell viability and thus mobility on day 7. (F) Slice 3 (bottom slice) showing no cell viability and thus no mobility through the alginate even on day 7. (G–L) inverted epifluorescent microscope images after live/dead staining of ADSCs on the collagen stacks. (G) Slice 1 (top slice) showing good cell viability on day 1. (H) Slice 2 (middle slice) showing good cell viability and therefore cells must be able to travel through on day 1. (I) Slice 3 (bottom slice) showing good cell viability and thus demonstrating the mobility of cells through the collagen and the micromachined fibre mesh even after 1 day. (J) Slice 1 (top slice) showing good cell viability on day 4. (K) Slice 2 (middle slice) showing good cell viability and therefore cells must be able to travel through on day 4. (L) Slice 3 (bottom slice) showing good cell viability and thus demonstrating the mobility of cells through the collagen and the micromachined fibre mesh on day 4. Scale bars: 500 µm. ADSC: adipose derived stem cell.

The next stage was to create a structure that is geometrically more complex, and to demonstrate the applicability of manufacturing technique for the purpose of creating scaffolds for use in maxillofacial and other surgical cosmesis procedures. At first, an ear with a height of approximately 50 mm was created successfully, with the different complex features of the ear prominent and clear. The next ear to be made was smaller at 28 mm tall, more akin to the size of a neonatal ear, and a third ear with a height of 38 mm was also constructed, both made using 0.2 mm thick paper slice. These demonstrators are shown in **Figure 2D**. One of the new challenges that came with fabricating the ear shape was that of the introduction of 2 different construct slices within one alignment slice, and the potential for loose sections that would be lost during the cutting process or wrongly attached to the structure. This was solved by adding more webs during the CAD process. The other new challenge comes from the fact that the cross-sectional area of ascending pieces increases in some parts of the construct. This increases the likelihood of unwanted adherence between the construct and the alignment slices, and also increases the likelihood of delamination when removing the alignment slices. This challenge can only be overcome by careful removal and, like before, better targeting of the application of alginate.

Using the thinner filter paper had the effect of reducing the layer height, a common method of increasing the resolution of a printed model. The ear in **Figure 2E** utilises filter paper that is half the thickness of the previous models. This has the effect of smoothing out the complex features of the ear. This has the drawback of doubling the length of time taken to fabricate the construct, which would have to be considered when this method is used to biomanufacture cell-laden scaffold constructs.

Morphological assessment of micromachined fibre meshes

From the SEM image of the electrospun nanofibre mesh, the average nanofibre diameter was found to be 1.801 µm. One study found that undifferentiated murine ADSCs have a diameter of 14.9 µm.47 Firstly, this is three times larger than

the average 'narrowest pore diameter' within the nanofibre mesh, indicating a need for micromachining to fulfill the desire for cell mobility through the mesh (and thus the construct). Secondly, it has been shown in literature that a mesh of nanofibres with a diameter smaller than the size of the cell has beneficial properties with respect to cell attachment and thus viability.[48] The diameter of the nanofibres is considerably smaller than the cells used, and such cell viability should be preserved.

It can be found in the literature that the process of micromachining holes into a fibre mesh can enhance the cell viability of the mesh.[41, 42] It is important in tissue engineering to have the construct mimic certain properties that are found in natural tissue ECM. Nanofiber meshes have good nanoporosity but further alterations are required in order to make it a more suitable mimic to that of bone ECM, for example. Micromachining is one such method used to achieve a better microporous representation, and as such improve the cell response within the scaffold.

Figure 4A–D clearly shows that the morphology of the micromachined holes created is uniformly rounded in shape, indicating a clean cut through from the nanosecond laser. This justifies the use of a nanosecond laser which ablates the polymer mesh through evaporation.[49] Analysis of the hole diameter also shows that the settings of the laser can be controlled in such a way as to accurately achieve the intended hole diameter. **Figure 5A** plots the actual average hole diameter against the intended diameter. It can be seen that the standard deviation (i.e. how round the hole is) increases as the hole diameter increases, suggesting that the round morphology is harder to control with the higher energies required to machine such a hole size.

It can be seen that the cells are surviving well on the array even well into the three-week time frame, and when left long enough the cells will attempt to 'bridge' even very large holes; by week 3 most 500 μm holes have been closed by the cells. Even with the large area of the holes which would account for dead space the confluence values are all calculated to be above 85%. This effect has promise for potential cell growth within these holes and vascularisation within the scaffold, a process that is vital for its success in the application of tissue engineering.

Viability of cells seeded in polycaprolactone and polylactic-co-glycolic acid three-dimensional scaffolds

It can be seen from **Figures 4I–K** and **5B** that the hole size is more difficult to control in the PCL electrospun fibre meshes used compared to the PLGA fibre meshes. This could be a result of the PCL fibre mesh having a more non-uniform thickness than the PLGA fibre mesh, meaning that the same parameters used for the micromachining process would produce inconsistent holes.

Comparing the two different adhesive types (alginate and collagen) showed that the stacks with cross linked alginate were less prone to delamination, especially surviving over longer cell culture conditions. The collagen samples, even though left for a sufficient time to thermally cross-link, were far more likely to break up and delaminate if not treated carefully. All samples maintained their shape by the end of the test.

As such, it can be said that the alginate adhesive provides better mechanical properties than the collagen adhesive, something to consider when potentially extrapolating this technique into the application of a bone graft.

It was initially hypothesised that the alginate would provide a barrier to any cell migration from the top of the stack through to the bottom due to its bioinert and dense properties (one reason why alginate is favoured in encapsulation applications for example[50]). Collagen however, with its bioactive properties was hypothesised to aid in cell migration through the stack. It was also hoped that the micromachined mesh would also aid cell migration.

The biofabricated construct is designed to be biomimetic whereby the 3D hierarchal structure found in natural human tissue such as bone and cartilage can be fabricated using this new approach. At a macro level, the biofabrication method is capable of creating anatomically accurate ear constructs of clinically relevant size. At the micro level, micromachining is implemented to enhance the microporosity properties to both aid cell migration through the construct and also help to replicate the natural porosity of bone ECM. At the nano level, the electrospun fibre mesh has already been shown to aid cell viability and proliferation due to its natural resemblance to natural tissue ECM.

Any cartilage or bone graft that would be utilised would have to be both mechanically and biologically sound, and biofabrication has a key role to play in the final implementation of such a successful, bespoke tissue engineered graft. The innovative biofabricated construct that is created utilises a wide range of techniques including electrospun nanofiber mesh, which is micromachined prior to assembly in a novel 3D fabrication method. This hierarchal construct can be described as having the potential to be both cosmetically accurate and induce a positive biological response. Different adhesives and cross-linking methods can be investigated to try to marry these two concepts. It is also important to broaden the cell types used and properly characterise the structures, something that will be achieved in future work.

Conclusion

This study has brought forth a novel and innovative way of fabricating a 3D hierarchical scaffold graft with good macro, micro and nanoscale precision, whilst also being able to utilise materials that have already shown promise within this application at the 2D level. At the macro level, the method of stacking 2D sheets of fibre mesh allows for bespoke grafts of clinically relevant sizes to be made, which would be of biocompatible and aesthetical benefit to any individual patient. At the micro level, it was found that the implementation of micromachined laser cut holes into each 2D slice provided an additional benefit to the graft by allowing for cell migration through the structure, by improving the microporosity of the fibre meshes. A replication of the nano level of the hierarchical structure was achieved by utilising nanofibre polymer meshes which have a similar morphology to the ECM of natural tissue. This study has also provided an insight into the role

of the adhesive used. Unsurprisingly, collagen proved to have better cell attachment, viability and migration however the stacks for which alginate was used as the binder provided better mechanical properties where delamination and adhesive degradation were less likely.

Further investigation is required into optimising the adhesive used so that it can be both mechanically and biologically suitable. The current adhesives used in this study both require optimisation in this regard. The capacity to involve better techniques of cell distribution using 3D bioprinting, the potential for the introduction of automation, as well as the wide range of model designs that can be achieved using such a fabrication method (to expand on the range of applications such as maxillofacial bone injury or nose/ear cartilage replacement) only adds to the promise.

Author contributions

WS and RHM conceived the idea and wrote the manuscript. RHM and WC designed and performed the experiments, with WC using the nanosecond laser. WS, BL, XL and RAB supervised the study. ZL, JW, FH, JW, XL and BL helped analyse the data and provided valuable advice. WS, RHM and RAB revised the manuscript. All authors approved the final version of the manuscript.

Financial support

The authors acknowledge the funding support from the EPSRC (Funding Reference Number EP/L015995/1 & EP/W004860/1), the Royal Society (IEC\NSFC\201166), the National Natural Science Foundation of China (No. 82111530157) and the Priority Academic Program Development (PAPD) of Jiangsu Higher Education Institutions.

Acknowledgement

We would like to thank Dr. Mathis Riehle University of Glasgow for the donation of ADSCs, Katie Henderson and Graeme MacKenzie in the SIPBS Department in the University of Strathclyde for Technical Assistance. We would like to thank the Electrospinning Company for donating the PLGA fibre meshes.

Conflicts of interest statement

None.

Editor note: Wenmiao Shu is an Editorial Board member of *Biomaterials Translational*. He was blinded from reviewing or making decisions on the manuscript. The article was subject to the journal's standard procedures, with peer review handled independently of this Editorial Board member and his research group.

1. Templer, J.; Renner, G. J. Injuries of the external ear. *Otolaryngol Clin North Am.* **1990**, *23*, 1003-1018.
2. Harris, J.; Källén, B.; Robert, E. The epidemiology of anotia and microtia. *J Med Genet.* **1996**, *33*, 809-813.
3. Gassner, R.; Tuli, T.; Hächl, O.; Rudisch, A.; Ulmer, H. Cranio-maxillofacial trauma: a 10 year review of 9,543 cases with 21,067 injuries. *J Craniomaxillofac Surg.* **2003**, *31*, 51-61.
4. Subhashraj, K.; Nandakumar, N.; Ravindran, C. Review of maxillofacial injuries in Chennai, India: a study of 2748 cases. *Br J Oral Maxillofac Surg.* **2007**, *45*, 637-639.
5. Turnbull, G.; Clarke, J.; Picard, F.; Riches, P.; Jia, L.; Han, F.; Li, B.; Shu, W. 3D bioactive composite scaffolds for bone tissue engineering. *Bioact Mater.* **2018**, *3*, 278-314.
6. Xu, L.; Qin, H.; Tan, J.; Cheng, Z.; Luo, X.; Tan, H.; Huang, W. Clinical study of 3D printed personalized prosthesis in the treatment of bone defect after pelvic tumor resection. *J Orthop Translat.* **2021**, *29*, 163-169.
7. Pu, F.; Wu, W.; Jing, D.; Yu, Y.; Peng, Y.; Liu, J.; Wu, Q.; Wang, B.; Zhang, Z.; Shao, Z. Three-dimensional-printed titanium prostheses with bone trabeculae enable mechanical-biological reconstruction after resection of bone tumours. *Biomater Transl.* **2022**, *3*, 134-141.
8. Long, J.; Teng, B.; Zhang, W.; Li, L.; Zhang, M.; Chen, Y.; Yao, Z.; Meng, X.; Wang, X.; Qin, L.; Lai, Y. Preclinical evaluation of acute systemic toxicity of magnesium incorporated poly(lactic-co-glycolic acid) porous scaffolds by three-dimensional printing. *Biomater Transl.* **2021**, *2*, 272-284.
9. Luquetti, D. V.; Leoncini, E.; Mastroiacovo, P. Microtia-anotia: a global review of prevalence rates. *Birth Defects Res A Clin Mol Teratol.* **2011**, *91*, 813-822.
10. Duscher, D.; Shiffman, M. A. *Regenerative medicine and plastic surgery*. Springer Nature Switzerland: Cham, Switzerland,2019.
11. Posnick, J. C. 18 - Grafts frequently used during orthognathic surgery and for adjunctive procedures. In *Orthognathic surgery*, Posnick, J. C., ed. W.B. Saunders: St. Louis, 2014; pp 607-639.
12. Elsalanty, M. E.; Genecov, D. G. Bone grafts in craniofacial surgery. *Craniomaxillofac Trauma Reconstr.* **2009**, *2*, 125-134.
13. Pacifici, L.; F, D. E. A.; Orefici, A.; Cielo, A. Metals used in maxillofacial surgery. *Oral Implantol (Rome).* **2016**, *9*, 107-111.
14. Sun, H.; Guo, Q.; Shi, C.; McWilliam, R. H.; Chen, J.; Zhu, C.; Han, F.; Zhou, P.; Yang, H.; Liu, J.; Sun, X.; Meng, B.; Shu, W.; Li, B. CD271 antibody-functionalized microspheres capable of selective recruitment of reparative endogenous stem cells for in situ bone regeneration. *Biomaterials.* **2022**, *280*, 121243.
15. Yang, T.; Tamaddon, M.; Jiang, L.; Wang, J.; Liu, Z.; Liu, Z.; Meng, H.; Hu, Y.; Gao, J.; Yang, X.; Zhao, Y.; Wang, Y.; Wang, A.; Wu, Q.; Liu, C.; Peng, J.; Sun, X.; Xue, Q. Bilayered scaffold with 3D printed stiff subchondral bony compartment to provide constant mechanical support for long-term cartilage regeneration. *J Orthop Translat.* **2021**, *30*, 112-121.
16. Yin, H. W.; Feng, J. T.; Yu, B. F.; Shen, Y. D.; Gu, Y. D.; Xu, W. D. 3D printing-assisted percutaneous fixation makes the surgery for scaphoid nonunion more accurate and less invasive. *J Orthop Translat.* **2020**, *24*, 138-143.
17. Li, D.; Xia, Y. Electrospinning of nanofibers: reinventing the wheel? *Adv Mater.* **2004**, *16*, 1151-1170.
18. Frenot, A.; Chronakis, I. S. Polymer nanofibers assembled by electrospinning. *Curr Opin Colloid Interface Sci.* **2003**, *8*, 64-75.
19. Tuzlakoglu, K.; Bolgen, N.; Salgado, A. J.; Gomes, M. E.; Piskin, E.; Reis, R. L. Nano- and micro-fiber combined scaffolds: a new architecture for bone tissue engineering. *J Mater Sci Mater Med.* **2005**, *16*, 1099-1104.
20. Sun, B.; Long, Y. Z.; Zhang, H. D.; Li, M. M.; Duvail, J. L.; Jiang, X. Y.; Yin, H. L. Advances in three-dimensional nanofibrous macrostructures via electrospinning. *Prog Polym Sci.* **2014**, *39*, 862-890.
21. Brown, T. D.; Dalton, P. D.; Hutmacher, D. W. Melt electrospinning today: an opportune time for an emerging polymer process. *Prog Polym Sci.* **2016**, *56*, 116-166.
22. Nayak, R.; Padhye, R.; Arnold, L. 2 - Melt-electrospinning of nanofibers. In *Electrospun nanofibers*, Afshari, M., ed. Woodhead Publishing: 2017; pp 11-40.
23. Zhang, L. H.; Duan, X. P.; Yan, X.; Yu, M.; Ning, X.; Zhao, Y.; Long, Y. Z. Recent advances in melt electrospinning. *RSC Adv.* **2016**, *6*, 53400-

53414.
24. Brown, T. D.; Edin, F.; Detta, N.; Skelton, A. D.; Hutmacher, D. W.; Dalton, P. D. Melt electrospinning of poly(ε-caprolactone) scaffolds: phenomenological observations associated with collection and direct writing. *Mater Sci Eng C Mater Biol Appl.* **2014**, *45*, 698-708.
25. Sun, W.; Starly, B.; Daly, A. C.; Burdick, J. A.; Groll, J.; Skeldon, G.; Shu, W.; Sakai, Y.; Shinohara, M.; Nishikawa, M.; Jang, J.; Cho, D. W.; Nie, M.; Takeuchi, S.; Ostrovidov, S.; Khademhosseini, A.; Kamm, R. D.; Mironov, V.; Moroni, L.; Ozbolat, I. T. The bioprinting roadmap. *Biofabrication.* **2020**, *12*, 022002.
26. Holmes, A. M.; Charlton, A.; Derby, B.; Ewart, L.; Scott, A.; Shu, W. Rising to the challenge: applying biofabrication approaches for better drug and chemical product development. *Biofabrication.* **2017**, *9*, 033001.
27. Holland, I.; Logan, J.; Shi, J.; McCormick, C.; Liu, D.; Shu, W. 3D biofabrication for tubular tissue engineering. *Biodes Manuf.* **2018**, *1*, 89-100.
28. Cornelissen, D. J.; Faulkner-Jones, A.; Shu, W. Current developments in 3D bioprinting for tissue engineering. *Curr Opin Biomed Eng.* **2017**, *2*, 76-82.
29. Sahranavard, M.; Sarkari, S.; Safavi, S.; Ghorbani, F. Three-dimensional bio-printing of decellularized extracellular matrix-based bio-inks for cartilage regeneration: a systematic review. *Biomater Transl.* **2022**, *3*, 105-115.
30. Turnbull, G.; Clarke, J.; Picard, F.; Zhang, W.; Riches, P.; Li, B.; Shu, W. 3D biofabrication for soft tissue and cartilage engineering. *Med Eng Phys.* **2020**, *82*, 13-39.
31. Groll, J.; Boland, T.; Blunk, T.; Burdick, J. A.; Cho, D. W.; Dalton, P. D.; Derby, B.; Forgacs, G.; Li, Q.; Mironov, V. A.; Moroni, L.; Nakamura, M.; Shu, W.; Takeuchi, S.; Vozzi, G.; Woodfield, T. B.; Xu, T.; Yoo, J. J.; Malda, J. Biofabrication: reappraising the definition of an evolving field. *Biofabrication.* **2016**, *8*, 013001.
32. Kang, H. W.; Lee, S. J.; Ko, I. K.; Kengla, C.; Yoo, J. J.; Atala, A. A 3D bioprinting system to produce human-scale tissue constructs with structural integrity. *Nat Biotechnol.* **2016**, *34*, 312-319.
33. Murphy, S. V.; Atala, A. 3D bioprinting of tissues and organs. *Nat Biotechnol.* **2014**, *32*, 773-785.
34. Wu, Z.; Su, X.; Xu, Y.; Kong, B.; Sun, W.; Mi, S. Bioprinting three-dimensional cell-laden tissue constructs with controllable degradation. *Sci Rep.* **2016**, *6*, 24474.
35. Yu, Y.; Hua, S.; Yang, M.; Fu, Z.; Teng, S.; Niu, K.; Zhao, Q.; Yi, C. Fabrication and characterization of electrospinning/3D printing bone tissue engineering scaffold. *RSC Adv.* **2016**, *6*, 110557-110565.
36. Gao, Q.; Gu, H.; Zhao, P.; Zhang, C.; Cao, M.; Fu, J.; He, Y. Fabrication of electrospun nanofibrous scaffolds with 3D controllable geometric shapes. *Mater Des.* **2018**, *157*, 159-169.
37. Gao, Q.; Zhao, P.; Zhou, R.; Wang, P.; Fu, J.; He, Y. Rapid assembling organ prototypes with controllable cell-laden multi-scale sheets. *Bio-des Manuf.* **2019**, *2*, 1-9.
38. Moroni, L.; Burdick, J. A.; Highley, C.; Lee, S. J.; Morimoto, Y.; Takeuchi, S.; Yoo, J. J. Biofabrication strategies for 3D in vitro models and regenerative medicine. *Nat Rev Mater.* **2018**, *3*, 21-37.
39. Dalton, P. D.; Woodfield, T. B. F.; Mironov, V.; Groll, J. Advances in hybrid fabrication toward hierarchical tissue constructs. *Adv Sci (Weinh).* **2020**, *7*, 1902953.
40. Sankar, S.; Sharma, C. S.; Rath, S. N.; Ramakrishna, S. Electrospun nanofibres to mimic natural hierarchical structure of tissues: application in musculoskeletal regeneration. *J Tissue Eng Regen Med.* **2018**, *12*, e604-e619.
41. Kong, B.; Sun, W.; Chen, G.; Tang, S.; Li, M.; Shao, Z.; Mi, S. Tissue-engineered cornea constructed with compressed collagen and laser-perforated electrospun mat. *Sci Rep.* **2017**, *7*, 970.
42. Lee, B. L.; Jeon, H.; Wang, A.; Yan, Z.; Yu, J.; Grigoropoulos, C.; Li, S. Femtosecond laser ablation enhances cell infiltration into three-dimensional electrospun scaffolds. *Acta Biomater.* **2012**, *8*, 2648-2658.
43. Aquino-Martínez, R.; Angelo, A. P.; Pujol, F. V. Calcium-containing scaffolds induce bone regeneration by regulating mesenchymal stem cell differentiation and migration. *Stem Cell Res Ther.* **2017**, *8*, 265.
44. Laco, F.; Grant, M. H.; Black, R. A. Collagen-nanofiber hydrogel composites promote contact guidance of human lymphatic microvascular endothelial cells and directed capillary tube formation. *J Biomed Mater Res A.* **2013**, *101*, 1787-1799.
45. Li, H.; Cheng, F.; Robledo-Lara, J. A.; Liao, J.; Wang, Z.; Zhang, Y. S. Fabrication of paper-based devices for in vitro tissue modeling. *Bio-des Manuf.* **2020**, *3*, 252-265.
46. Moe, S. T.; Skjaak-Braek, G.; Elgsaeter, A.; Smidsroed, O. Swelling of covalently crosslinked alginate gels: influence of ionic solutes and nonpolar solvents. *Macromolecules.* **1993**, *26*, 3589-3597.
47. No authors listed. Rapid analysis of human adipose-derived stem cells and 3T3-L1 differentiation towards adipocytes using the Scepter™ 2.0 Cell Counter. *Biotechniques.* **2012**, *53*, 2.
48. Laurencin, C. T.; Ambrosio, A. M.; Borden, M. D.; Cooper, J. A., Jr. Tissue engineering: orthopedic applications. *Annu Rev Biomed Eng.* **1999**, *1*, 19-46.
49. Bridle, H.; Wang, W.; Gavriilidou, D.; Amalou, F.; Hand, D. P.; Shu, W. Static mode microfluidic cantilevers for detection of waterborne pathogens. *Sens Actuators A Phys.* **2016**, *247*, 144-149.
50. Faulkner-Jones, A.; Fyfe, C.; Cornelissen, D. J.; Gardner, J.; King, J.; Courtney, A.; Shu, W. Bioprinting of human pluripotent stem cells and their directed differentiation into hepatocyte-like cells for the generation of mini-livers in 3D. *Biofabrication.* **2015**, *7*, 044102.

Received: January 27, 2023
Revised: April 19, 2023
Accepted: June 20, 2023
Available online: June 28, 2023